

# Stereoselectivity in Asymmetric Catalysis: The Case of Ruthenium-Catalyzed Ketone Hydrogenation

Elaine Limé,<sup>†,‡</sup> Michelle D. Lundholm,<sup>§</sup> Aaron Forbes,<sup>§</sup> Olaf Wiest,<sup>§,||</sup> Paul Helquist,<sup>§</sup> and Per-Ola Norrby<sup>\*,†,‡</sup>

<sup>†</sup>Department of Chemistry and Molecular Biology, University of Gothenburg, Kemigården 4, SE-412 96 Göteborg, Sweden

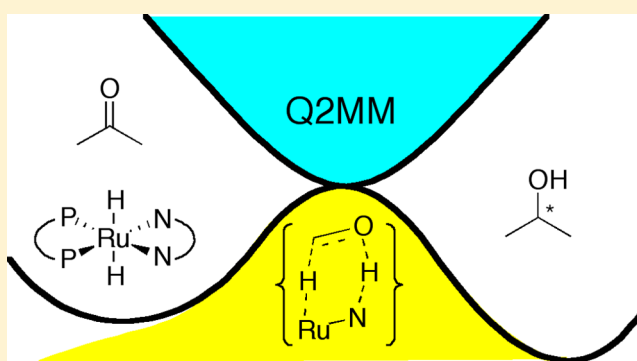
<sup>‡</sup>Pharmaceutical Development, Global Medicines Development, AstraZeneca, Pepparedsleden 1, SE-431 83 Mölndal, Sweden

<sup>§</sup>Department of Chemistry and Biochemistry, University of Notre Dame, Notre Dame, Indiana 46556 United States

<sup>||</sup>Lab of Computational Chemistry and Drug Design, Laboratory of Chemical Genomics, Peking University Shenzhen Graduate School, Shenzhen 518055, China

## S Supporting Information

**ABSTRACT:** The ruthenium-catalyzed asymmetric hydrogenation of simple ketones to generate enantiopure alcohols is an important process widely used in the fine chemical, pharmaceutical, fragrance, and flavor industries. Chiral diphosphine–RuCl<sub>2</sub>–1,2-diamine complexes are effective catalysts for the reaction giving high chemo- and enantioselectivity. However, no diphosphine–RuCl<sub>2</sub>–1,2-diamine complex has yet been discovered that is universal for all kinds of ketone substrates, and the ligands must be carefully chosen for each substrate. The procedure of finding the best ligands for a specific substrate can be facilitated by using virtual screening as a complement to the traditional experimental screening of catalyst libraries. We have generated a transition state force field (TSFF) for the ruthenium-catalyzed asymmetric hydrogenation of simple ketones using an improved Q2MM method. The developed TSFF can predict the enantioselectivity for 13 catalytic systems taken from the literature, with a mean unsigned error of 2.7 kJ/mol.



## INTRODUCTION

One of the holy grails of computational chemistry is to achieve the status of a predictive science. In the ideal scenario, new chemical reactions would be designed *in silico* before actual implementation in the laboratory. Quantum mechanical (QM) theories are slowly attaining the accuracy where this could become possible. In practice, the multitude of possible pathways coupled with the computational demand of QM calculations makes the task daunting, even though promising approaches have been demonstrated.<sup>1</sup> For the more limited task of predicting the effect of variation of a given reaction to achieve better yields and selectivities, where a significant part of the effort in organic chemistry is spent, the picture is much brighter.

Computational methods for calculation of chemical reactivity and selectivity can be roughly divided into those that are trained using known data and those that achieve the prediction by direct modeling without recourse to experimental observations. The former methods include quantitative structure–reactivity relationships (QSRR)<sup>2</sup> but also approaches like molecular mechanics force fields trained on experimental data to reproduce a specific type of selectivity.<sup>3,4</sup> The latter methods are based on direct modeling and are more

demanding in that, in principle, all possible reaction pathways must be calculated and compared. However, success with such methods is very satisfying in that it demonstrates a thorough understanding of the reaction mechanism, as well as a high accuracy in the modeling of all interactions of importance to the question under study.

We are interested in applying the direct modeling approach in the area of asymmetric catalysis.<sup>5</sup> To achieve our goals in this area, we must accurately model bonds and possibly bond breaking involving transition metals, as well as long-range interactions and multiple conformations of the selectivity-determining transition state (TS). On the other hand, the selectivity in many cases is fully determined in one unique step. In such cases, the problem is simplified because the reactant ensemble is the same for both possible stereoisomeric products and thus can be excluded from the modeling. Therefore, only the relative energies of closely related, diastomeric transition states contribute to the final selectivity. Our ultimate goal is to allow reliable virtual screening, which would entail investigating several thousand variations of one reaction (*e.g.*, a ligand screen

Received: February 28, 2014

Published: May 14, 2014

for one particular substrate), for a system size where each variation might require screening of up to 1 million transition state conformations, resulting in billions of structure optimizations for each screen.

Direct modeling methods of selectivity can be based on QM or molecular mechanics (MM) methods (Figure 1), or a

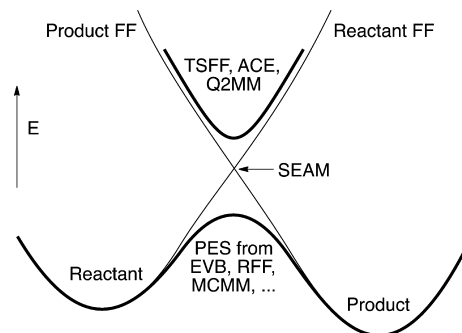


Figure 1. Various MM approaches to TS modeling.

combination of both.<sup>6</sup> MM methods are several orders of magnitude faster than QM but can be limited by the availability of properly determined force field parameters. Application of QM to modeling of all possible transition states of a reaction is still limited to relatively small and rigid systems<sup>1</sup> due to the CPU requirements of QM methods, even though the boundaries in this field are pushed back yearly and more and more systems become amenable to this approach. Higher efficiencies can be obtained with QM/MM approaches, where the conformational screening of different pathways can be done largely in the classically treated MM region.<sup>7</sup> Still, the most extensive calculations of this type in the literature do not screen more than a few thousand distinct TSs, mainly due to the manual effort required in ensuring proper convergence in each case. Pure MM approaches are fast enough to allow determination of the millions of TSs needed in a virtual screen. Any MM method that simulates a true potential energy surface (PES)<sup>4,8</sup> will still suffer from the requirement to converge to or sample appropriately at saddle points on the PES, nontrivial tasks that have not yet been fully automated. A few MM approaches, notably the EVB model potential,<sup>4</sup> SEAM,<sup>9</sup> ACE,<sup>10</sup> TSFF,<sup>3</sup> and our own Q2MM<sup>11</sup> method allow direct optimization to approximate transition states by reliable minimization procedures.<sup>12</sup> These can therefore be incorporated into virtual screening schemes, employing a well established sampling method to find all TS conformations for a given reaction path.

Currently, the most accurate method for predicting stereoselectivities is the Q2MM method.<sup>13</sup> The Q2MM force field for the asymmetric dihydroxylation reaction, originally released in 1999, has been applied to a wide range of substrates and ligands with a mean unsigned error (MUE) of 2.5 kJ/mol over all published examples.<sup>14</sup> We note that this is significantly better than the anecdotal “1 kcal/mol” that is frequently stated as a desired target for molecular modeling accuracy and in the range required for the reliable identification of highly stereoselective reactions. The total set of dihydroxylation predictions comprises 27 different substrate–ligand combinations and required approximately 1 million conformational energy evaluations. Today, this computational task requires about a day on a commodity workstation. The Q2MM method has also been applied to the rhodium catalyzed asymmetric hydro-

genation of enamides,<sup>15</sup> yielding a MUE of 3.2 kJ/mol over 29 examples (Figure 2).

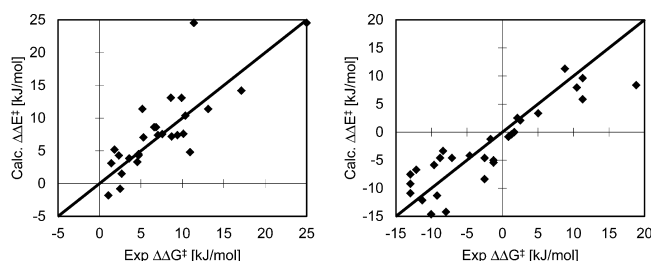
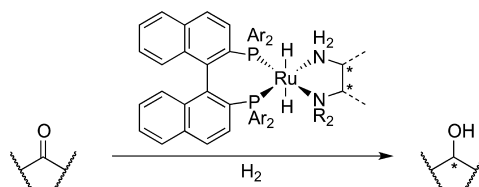


Figure 2. Calculated vs experimental enantioselectivity for the dihydroxylation<sup>14</sup> (left) and hydrogenation reactions<sup>15</sup> (right).

Here, we have updated the Q2MM method and applied it to Ru-catalyzed asymmetric hydrogenation of ketones, Scheme 1,

### Scheme 1. Noyori Catalyst for Asymmetric Hydrogenation of Ketones



which has been developed to a high state of refinement by Noyori and coworkers.<sup>16,17</sup> This reaction has several features that make it highly suitable for a Q2MM approach. It is a synthetically important transformation, allowing chemo- and stereoselective reduction of ketones to alcohols. The target chiral alcohols represent ubiquitous structural elements in natural products as well as in drug and drug-like molecules. Many chiral reagents can reduce ketones, but only a small class of transition metal catalysts can utilize inexpensive hydrogen gas as the stoichiometric reducing agent. The reaction has been extensively studied by quantum chemical methods, and the mechanism is well understood.<sup>18,19</sup> A single, well-characterized step determines the stereoselectivity in the reaction. Furthermore, the catalyst is modular, containing two independent chiral ligands, a diphosphine and a diamine. It has been shown that proper selection of the two ligands can allow high yield and selectivity for a wide range of substrates. The preferred enantiomer can usually be rationalized by an orientation wherein the carbonyl oxygen interacts with an axial N–H, and the smaller ketone substituent is oriented toward the bulky diphosphine (Figure 3),<sup>20</sup> but no general rule has been found to allow an *a priori* selection of the best combination of diphosphine and diamine ligands to be employed with a given ketone substrate. As a result, the combinatorics of possible diphosphine and diamine ligands is a formidable task for

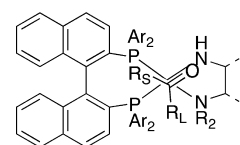


Figure 3. Preferred TS in the ketone hydrogenation.  $R_S$  = small,  $R_L$  = large.

experimental screening approaches. A fast computational preselection of the most promising pairs of ligands could significantly reduce the experimental effort needed for finding the optimum catalyst for any given substrate.

## COMPUTATIONAL DETAILS

The Q2MM method has been described in the literature.<sup>11,13</sup> In brief, the selectivity-determining step is calculated for several small model systems with a suitable QM method. The identical systems are calculated with a TSFF using preliminary trial parameters. The parameters are then varied until maximum correspondence between the QM and MM models has been achieved. The key to the Q2MM method lies in the handling of the calculated vibrational data. The QM vibrational analysis uniquely describes a saddle point, having one negative eigenvalue in the mass-weighted Hessian matrix. The single negative eigenvalue, corresponding to the reaction coordinate, must be modified to a large positive value before the data are used in the parametrization.<sup>21</sup> Forcing the MM to reproduce the now positive definite Hessian matrix at what is in reality a transition structure automatically gives a force field that treats the TS as if it were an energy minimum.

**Calculation of the QM Training Set.** All quantum mechanical calculations were performed using Becke's three parameter hybrid-generalized gradient approximation (GGA) density functional (B3LYP)<sup>22</sup> with the lacvp\* basis set as implemented in Jaguar 7.9.<sup>23</sup> The lacvp\* basis set uses an effective core potential (ECP) to describe the inner core electrons for ruthenium, and the outer electrons were described by a valence double- $\zeta$  basis set (LANL2DZ).<sup>24</sup> All other atoms were described by the 6-31G\* basis set. All TS structures were fully optimized and characterized with vibrational analysis verifying that the TSs had one imaginary frequency corresponding to the reaction coordinate. ESP charges<sup>25</sup> were constrained to reproduce the overall molecular dipole moment, and also to specific atomic charges as described later.

Seven different TS models were calculated (Table 1). The diphosphine ligand was modeled as (1Z,3Z)-1,3-butadiene-1,4-

**Table 1. Ru Complexes with Different Diamines and Substrates**

diamine	substrate
ethane-1,2-diamine A1	acetone S1
ethane-1,2-diamine A1	acetophenone S2
ethane-1,2-diamine A1	cyclopentenylethanone conf 1 S3a
ethane-1,2-diamine A1	cyclopentenylethanone conf 2 S3b
N,N-dimethylethane-1,2-diamine A2	acetophenone S2
(2S,3S)-butane-2,3-diamine (2S,3S)-A3	acetone S1
(2S,3S)-butane-2,3-diamine (2S,3S)-A3	acetophenone S2

diphosphine in all cases. Three different diamines and ketones were utilized in the training set (Figure 4). When there was a conformational choice, the smaller ketone substituent was positioned over the diphosphine moiety.

**Parameter Refinement.** Using the Q2MM method,<sup>13</sup> the parameters are refined by minimizing a penalty function,  $\chi^2$ . This function is defined as the square of the sum of the differences between the QM-calculated data points in the reference set and the MM corresponding values given by a specific force field, eq 1. These sums are weighted depending on the type of reference data (Table 2). Weighting factors were chosen on the principle of "the inverse of the acceptable

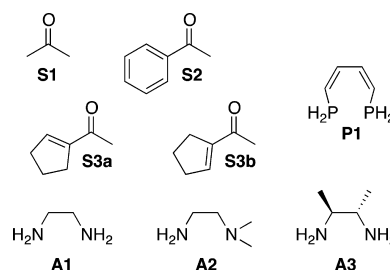


**Figure 4.** Substrates, diphosphine, and diamines used in the training sets. Two different rotamers of cyclopentenylethanone were included, S3a and S3b.

**Table 2. Weighting Factors for the Different Types of Reference Data**

type of reference data	weighting factor ( $w_i$ )
charges [ $e^{-1}$ ]:	
ruthenium	1
other elements	30
united atom charges <sup>a</sup>	100
bond lengths [ $\text{\AA}^{-1}$ ]	100
bond angles [ $\text{degree}^{-1}$ ]	2
inverse distances [ $\text{\AA}$ ]	4
relative energies [ $\text{kJ}^{-1} \text{mol}$ ]	10
forces [ $\text{kJ}^{-1} \text{mol \AA}$ ]	0.03
mass-weighted Hessian elements [ $\text{kJ}^{-1} \text{mol \AA}^2 \text{amu}^{-1}$ ]:	
block diagonal <sup>b</sup>	0.0
between atoms separated by 1 bond	0.02
between atoms separated by 2 bonds	0.04
between atoms separated by 3 bonds	0.10
other	0.01

<sup>a</sup>Sum of charges for atoms with attached hydrogens. <sup>b</sup>Hessian elements with both coordinates on the same atom.

error,"<sup>26</sup> with units making the final penalty function unitless. The relative weights of Hessian elements are based on the work by Hagler and co-workers.<sup>27</sup> However, a significant difference from earlier versions of Q2MM is that block-diagonal elements (i.e., single atom Hessian elements) are removed, that is, the corresponding  $w_i$ 's are set to zero, as discussed in detail in the Optimization of Force Constants section (*vide infra*). A combination of alternating modified Newton–Raphson and Simplex optimizations is used to minimize the penalty function,<sup>28</sup> which is arbitrarily considered to be converged when it is improved by less than 0.01% between two consecutive steps.

$$\chi^2 = \sum_i w_i^2 (y_i^{\text{QM}} - y_i^{\text{MM}})^2 \quad (1)$$

**Test Set Conformational Search.** The mixed Monte Carlo<sup>29</sup>/Low Mode<sup>30</sup> method in MacroModel<sup>31</sup> was used for the conformational searches. Between 1000 and 200 000 steps were used for each diastereomeric transition structure depending on the number of freely rotatable bonds. For each search, whenever a new global minimum was located within the second half of the search, the number of steps was doubled. The reaction channels to R and S products were calculated separately. The energy difference between the Boltzmann ensembles for each channel gave  $\Delta\Delta E^\ddagger$  (eq 2), which was compared to the experimental  $\Delta\Delta G^\ddagger$  obtained from the reported e.e. or e.r. for each reaction. The energies derived from

the Boltzmann ensembles differed only slightly from taking the difference between the lowest energy conformer from each reaction channel (see Supporting Information). We note that the current treatment utilizes the common molecular mechanics assumption that  $\Delta\Delta E^\ddagger \approx \Delta\Delta H^\ddagger$  and also assumes that only the conformational entropy difference contributes to the selectivity (i.e., that solvation and vibrations do not contribute significantly to the difference between diastereomeric paths).

$$\Delta\Delta E^\ddagger = RT \ln \left( \frac{\sum_{\text{pro-R}} e^{-\Delta E_i/RT}}{\sum_{\text{pro-S}} e^{-\Delta E_i/RT}} \right) \quad (2)$$

## ■ RESULT AND DISCUSSION

**Training Set.** The seven transition state searches gave structures that are in close agreement with previous computational studies of the reaction.<sup>18–20</sup> The carbonyl C=O and the reacting Ru–H and N–H bonds all lie close to a common plane. The average bond distances, listed in Table 3, indicate

**Table 3. QM Average Bond Lengths for Ru and for Atoms Involved in the TS Ring**

bond	average length [Å]	std. dev.
Ru–P	2.27	0.005
Ru–H <sub>spectator</sub>	1.68	0.007
Ru–H <sub>TS</sub>	1.77	0.017
Ru–N <sub>spectator</sub>	2.24	0.040
Ru–N <sub>TS</sub>	2.19	0.004
N–H	1.04	0.003
H···O	1.84	0.034
C=O	1.25	0.005
C···H	1.80	0.056

early, reactant-like transition states. The Ru distances to the two hydrides are similar, with the reacting Ru–H bond only ca. 0.1 Å longer than the spectator Ru–H bond. The N–H···O interaction can be described as a hydrogen bond, with N–H ca. 1.04 Å and H···O ca. 1.84 Å.<sup>19</sup> The carbonyl C=O is only slightly elongated, and the transferring hydride is still ca. 1.8 Å from the carbonyl carbon. The seven transition states show consistent bond lengths, with only a few hundredths of an ångström variation (Table 3). The angles all fall fairly close to expected values but show a bit more variation, with standard deviations in some cases exceeding 1° (Table 4). It can be

**Table 4. QM Average Bond Angles Involved in the TS Ring and around the Ru Atom**

angle	average angle [deg]	std dev.
Ru–N <sub>TS</sub> –H <sub>TS</sub>	105.3	0.331
Ru–H···C	146.6	0.557
N–H···O	153.6	1.502
H···O=C	107.0	1.099
O=C···H	107.6	0.659
N <sub>TS</sub> –Ru–H <sub>TS</sub>	85.1	0.562
H–Ru–H	174.5	0.321
P–Ru–N <sub>spectator</sub> (trans)	173.9	0.763
P–Ru–N <sub>spectator</sub> (cis)	96.6	0.335
P–Ru–N <sub>TS</sub> (trans)	175.1	0.951
P–Ru–N <sub>TS</sub> (cis)	96.6	0.818

noted that the angles across the transferring hydride and proton, which would be expected to be close to 180° in open transition states, are constrained by the six-membered ring transition states to values closer to 150° (Table 4).

The A1–S2 combination of diamine ligand and substrate was used to investigate the different isomers of the TS. The two bidentate ligands will both have two possible *gauche* conformations, giving either  $\lambda$  or  $\delta$  coordination to Ru, resulting in two possible diastereomers of the TS. We have included both the  $\lambda,\lambda$ - and  $\lambda,\delta$ -structures to represent both matched and mismatched ligand combinations. Each of these was calculated with the aryl moiety of the S2 substrate oriented either toward the diamine or toward the diphosphine moiety, giving four isomeric TS structures for A1–S2 and thus a total of 10 structures in the extended training set.

Structures having the substrate oxygen interacting with the equatorial amino hydrogen were also calculated. These structures are less favorable than those in which the substrate interacts with the axial amino hydrogen and were only used in the validation of the final force field.

**Preparation of the MM3\* Force Field.** The MM3 force field<sup>32</sup> as implemented in MacroModel<sup>31</sup> (termed MM3\*) was used as the foundation of the calculations. Parameters for the Ru environment and the TS structure were added to this force field. The van der Waals (vdW) radius and hardness for Ru were taken from published MM3 parameters<sup>33</sup> and used without further refinement. Most atoms are given common atom types to allow maximum utilization of existing ground state parameters outside the redefinition set. However, it was necessary to use a nonstandard atom type for the transferring hydride, since MacroModel applies an offset to all recognized hydrogens based on the assumption that hydrogen atoms always are terminal. The MacroModel atom and bond types used for the definition of new parameters in the reaction center are depicted in Figure 5. The P–Ru–N angles can be either *cis*

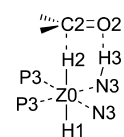


**Figure 5.** MacroModel atom types and bond orders used in the definition of new parameters. Z0 is the generic metal type, and zero order bonds are represented by dashes.

or *trans* and are handled by the MacroModel function for geometry dependent parameters. Different sets of angle parameters are used depending on whether the value of the angle in the starting structure is larger or smaller than 135°. Other parameters for the phosphorus atoms are identical, whereas the two nitrogen atoms are differentiated.

Existing ground state parameters were utilized as far as possible, but in cases where the environment has significantly changed (e.g., for any O2=C2–C bending parameters), new parameters are generated in the refinement. A full list of all parameters included in the refinement can be found in the Supporting Information.

Initial trial values for new bond and angle parameters were set to the average values obtained from the training set of QM structures listed in Tables 3 and 4. Force constants were initially set to standard values for bonds and angles, 5 mdyn/Å and 0.5 mdyn/rad, respectively. Initial torsional parameters were set to zero. For angles with reference values close to but



not identical to  $180^\circ$ , an energy cusp at  $180^\circ$  leads to convergence problems with these parameters. The *trans* angles (P–Ru–N and H–Ru–H) were therefore given a reference value of exactly  $180^\circ$  and a force constant of 0.25 mdyne/rad and were left out of the parameter refinement.

**Optimization of Electrostatic Parameters.** The original MM3 force field uses an electrostatic bond model based on bond dipoles. The MM3\* force field utilizes the MM3 bond dipole parameters but uses them internally only to set appropriate atomic charges of the two atoms connected by the bond. In the current parameter refinement, the bond dipole parameters have been refined to achieve the best possible fit between MM3\* atomic charges and DFT-calculated ESP charges.<sup>25</sup> As before,<sup>13</sup> we have compared both atomic charges and, with a higher weight, united atom charges where the hydrogen charges were added to the attached atom. Because the ESP protocol gives the most reliable charges for the surface atoms, the deeply buried Ru atom has been given a low weight in the fitting (Table 2). The initial training set of seven structures was split into a charge training set of three complexes (A1–S2, A1–S3a, and A3–S2) and a charge validation set of the remaining four structures (Table 1 and Figure 4).

The set of QM structures includes a number of atomic charges that are not affected by the refined parameters. To avoid unbalancing effects at the interface between reparameterized and original charges, the QM calculations were constrained to the MM3\* values when determining the ESP charges using the atomic section specification options in Jaguar.<sup>23</sup> Details about these constraints can be found in the Supporting Information. In short, all aliphatic hydrogens and aliphatic carbons only bound to hydrogen and other aliphatic carbons were constrained to a zero charge, whereas aromatic and vinylic C–H moieties were constrained to  $-0.113$  on C and  $0.113$  on H. The ESP charges were also constrained to reproduce the molecular dipole.

The charge parameters (“bond dipoles”) were first given reasonable starting values by manual adjustment on a bond-by-bond basis. The full set of charge parameters was then optimized using a penalty function consisting only of ESP charges (Table 2, rows 1–3). It is not possible to achieve a perfect fit because atoms that are isoparametric in the force field will have different charges in the QM calculation. The final result is depicted in Figure 6. Each set of isoparametric atom charges appears as a horizontal line of dots and is well centered on the diagonal (Figure 6, left). Reassuringly, the validation set gave a fit of only slightly lower quality (Figure 6, right). The final charges were fixed at this point and not further refined.

**Optimization of the Force Constants.** We next optimized the force constants using an approach that differs

from the earlier implementations and will therefore be discussed in some detail. Force constants are the second derivative of the energy with respect to a structural parameter. These are best determined by fitting to Hessian elements, that is, the full matrix of second derivatives of the energy with respect to Cartesian coordinates. For a TSFF, the Hessian data must be modified, since the Hessian matrix for a TS will always have one negative eigenvalue (a saddle point on the energy surface), whereas the TSFF should have only positive eigenvalues (corresponding to an energy minimum). In the Q2MM method, the mass-weighted Hessian is diagonalized, and the negative eigenvalue is replaced by a large positive value, whereupon the modified Hessian is reformed from the eigenvectors and eigenvalues.<sup>21</sup> Thus, the original and modified Hessians will have identical eigenvectors, but will differ in one eigenvalue.

A Hessian element relates two coordinates in the molecule and can best be visualized as the change in force on one atom upon a small displacement of either the same or a different atom. Bond force constants will be reflected in Hessian elements for atoms separated by one bond, whereas angle force constants affect atoms separated by one or two bonds. At longer connectivity distances, atoms are affected by torsional functions (up to three bonds) and nonbonded forces (vdW and electrostatic interactions, at least three-bond separations in MM3-type force fields). To reflect the different nature of the Hessian elements, they are scaled with weight factors inspired by the work of Hagler and co-workers<sup>27</sup> (Table 2). Block-diagonal Hessian elements, that is, derivatives with respect to two coordinates on the same atom, do not correspond directly to any MM interactions but are instead linearly dependent on all other Hessian elements. Since they do not contribute any additional information to the parametrization, they have been removed in the current refinement by setting the corresponding weight factors to zero.

Not all elements of a QM Hessian can be adequately reproduced by standard force fields. For example, there are no force field terms that reproduce the coupling when atoms separated by more than three bonds are in conjugation. Even for the three-bond separation, only vectors that correspond to torsional movements or vdW interactions can be reproduced. In transition states with concerted bond breaking and forming in different parts of the molecule, this problem is particularly pronounced, and the deviations become more noticeable since the reaction coordinate has been modified to have a large positive eigenvalue. The effect will be that displacements along the reaction coordinate will give an incorrect energy change in the force field. However, such displacements are minimized by the large eigenvalue, and furthermore, the errors are systematic, applying similarly to all competing pathways. Thus, the incomplete reproduction of Hessian elements connected to the reaction coordinate seems to have little effect on the final predictive power of the Q2MM force fields.<sup>5,13</sup>

Hagler and co-workers have suggested a parameter optimization method whereby the penalty function contains only energies, forces, and Hessian elements.<sup>27</sup> However, in our experience, this leads to convergence problems for Q2MM force fields for which only stationary points can be included in the training set. Some force constants tend toward zero, which can lead to an unstable force field. We therefore augment the penalty function by also including structural data for optimized structures.<sup>28</sup>

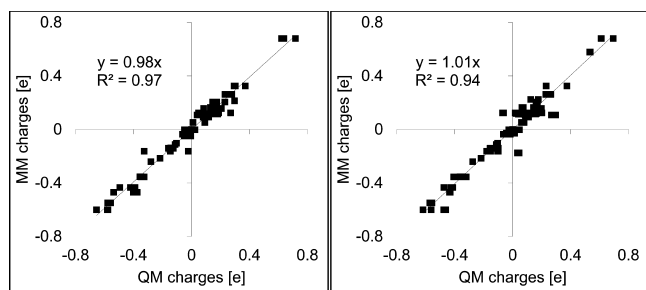


**Figure 6.** Left: three-structure charge training set. Right: four-structure charge validation set.

The use of structural data in the penalty function leads to some interdependence between parameters, which in turn can give convergence problems in the refinement. Problematic parameter sets could be detected by strong deviation of reference bonds and angles from the observed values in the training set, or by very low force constants, indicating nonphysical local minima in the penalty functions. To circumvent these problems, we initially optimized the parameters in subsets. We also initially added terms to the penalty function where deviations from the initial guesses were penalized by a harmonic constraint, referred to as tethering. However, the final refinement included all parameters and no tethering, showing that the final force field is a local optimum for the penalty function.

**Optimization of Torsional Parameters.** In MM, torsional parameters are generally seen as correction terms, for example to handle orbital overlaps in 1,4-interactions not covered by nonbonded interactions. The MM3 torsional terms can be seen as the three leading terms of a Fourier expansion of the difference between a real torsional profile and the MM profile in the absence of torsional terms.<sup>34</sup> In principle, determination of all torsional parameters requires a full sampling over a 360° bond rotation. However, in constricted structures like the TS considered here, only a narrow section of the full rotational profile is relevant, leading to a strong linear dependence between the possible torsional parameters. Thus, only one term was selected to be optimized for most torsions, based on the symmetry of the expected dominant interaction and the observed values in the training set structures. Unused torsional parameters were set to zero. For the bonds to the octahedral metal, a 4-fold torsional term was included. We also included the improper torsion describing the planarity of the carbonyl, since this is expected to change drastically in a reaction going from the  $sp^2$  carbonyl to the  $sp^3$  carbon in an alcohol.

For each final torsional parameter, the relevance of the value was considered. If the converged parameter had a low value, we tested whether it could be set to zero without significant worsening of the penalty function. If so, it was removed from the set and from further refinement.

**Optimization of the Structural Parameters.** The reference values for bond lengths and angles are “ideal” values that can differ from the values seen at equilibrium. Only in a theoretical “unstrained” structure would the values match exactly. However, the energy penalty associated with deviation from the reference value generally ensures that the equilibrium values stay close to the ideal, especially for bonds that generally have strong force constants. Thus, large deviations between the reference and observed values can usually be seen as an indication of problematic parameter refinement. Two types of data points in the penalty function are strongly affected by the structural parameters: the training set values for bonds and angles and the forces on atoms for single point MM calculations on the training set. The latter are also dependent on the already optimized force constants and thus introduce a linear dependence in the parameter optimization. Thus, the structural parameters were initially refined alone, without changing the force constants or torsional parameters, first with tethering to the observed values, then without tethering.

**Global Optimization.** After optimization of the structural parameters, all parameters were subjected to a global refinement, with the exception of electrostatic parameters and the parameters for the *trans* angles (*vide supra*). At this point, we added the relative energies of four conformers of A1–S2

(Figure 4) to the penalty function and excluded only the charge data (Table 2). The final values of all parameters can be found in the Supporting Information.

**Internal Validation.** The success of the parameter refinement was first evaluated by the ability of the final force field to reproduce the data used in the penalty function. The charge data that have already been discussed (Figure 6) illustrate that the trend is well reproduced, but individual variations among isoparametric atoms cannot be fully reproduced by the force field. The bond and angle agreement shows excellent correspondence, Figure 7. Residual plots for bond lengths and angles can be found in the Supporting Information.

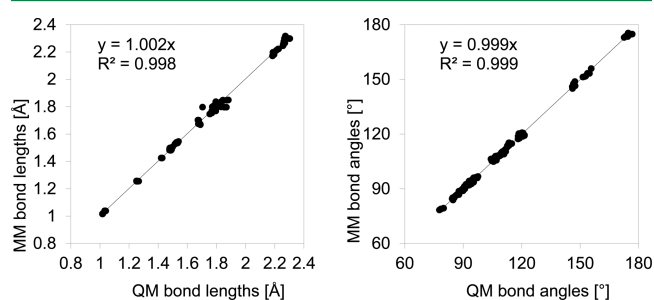


**Figure 7.** Internal validation of 170 bond lengths (left) and 245 angles (right).

The comparison of weighted Hessian elements can be seen in Figure 8. These values show bimodal behavior, as is

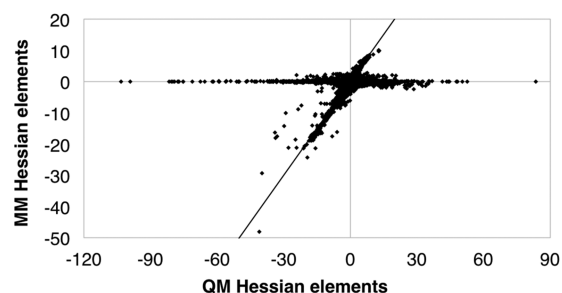


**Figure 8.** Comparison of Hessian elements, weighted according to Table 2.

commonly observed for Q2MM force fields. Values that are well reproduced by the force field are aligned along the diagonal. The values on the  $x$  axis are Hessian matrix elements corresponding to interactions that are ignored by the force field, as discussed earlier (*vide supra*). The scaled Hessian values depicted in Figure 8 are unitless but have a range of ca. 60 in the MM regime and 200 in the QM regime. We can analyze the data in terms of an arbitrarily chosen error limit of 3, which corresponds to 5% of the MM range and 1.5% of the QM range. We can then see that 67 852 of the 70 188 Hessian elements depicted in Figure 8 fall on the diagonal, within our error limit. A further 2281 elements fall on the  $x$  axis, as already discussed, and only 55 elements are outliers of another type. The latter correspond to interactions that can, to some extent, be represented by a force field but are not well fitted. One such example is shown in Figure 9. The C and H atoms are bonded in the force field, but the bonding interaction can only give rise to Hessian elements that are parallel to the bond vector. Here, the vector on H is perpendicular to the C–H “bond.” This

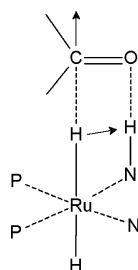


Figure 9. Example of an outlier Hessian element (Figure 8).

Hessian element will get a nonzero value from any angle including both atoms, but the value cannot be reproduced without upsetting the balance for the other Hessian elements affected by the same angle. From inspection of representative elements, these outliers are in most cases connected to displacements along the reaction coordinate. Within the constraints of the chosen functional form, we cannot address this problem, but such displacements will, in actual usage, be minimized by the high force constant chosen for the reaction coordinate eigenvector, and thus should have little influence on relative energies of similar transition states.

**External Validation.** The final force field was validated against a test set of experimental enantioselectivities for ligand–substrate combinations shown in Figure 10 and Table 5. As outlined in the computational details, each substrate–ligand combination was subjected to extensive conformational searching for each diastereomeric path. The final  $\Delta\Delta E^\ddagger$  is the energy difference between the Boltzmann ensembles over the different diastereomeric paths. The results are shown together with literature values in Table 5. If we instead calculate  $\Delta\Delta E^\ddagger$  as the energy difference between the lowest energy structures leading to either enantiomer of the product, the predictions change somewhat, but the overall quality remains similar (see the Supporting Information for comparison).

As can be seen in Figure 11, the correspondence between experimental and computational data is excellent, with a MUE of only 2.7 kJ/mol. This is comparable to predictions from QSAR approaches where the models have been based on experimental data.<sup>2</sup> It should be emphasized that the current Q2MM model is built solely on QM data and thus was created without recourse to experiments. An error of 2 kJ/mol corresponds to a factor of 2 in relative predicted populations. For example, a prediction of 98% selectivity with an error of 2 kJ/mol would correspond to a real selectivity in the range 96–

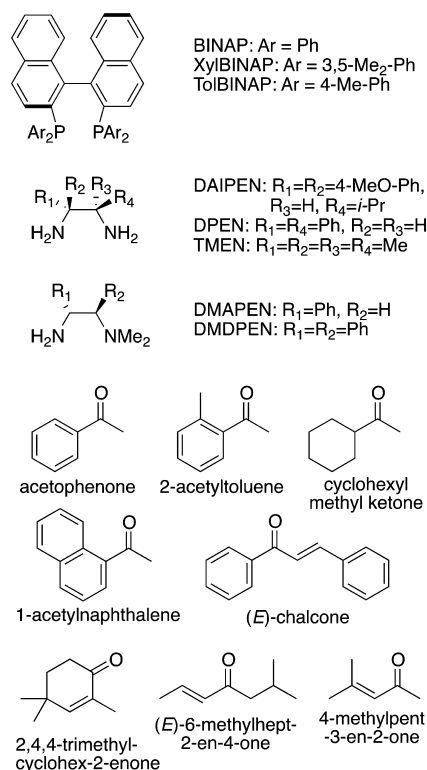


Figure 10. Diphosphines, diamines, and substrates used in the validation test set.

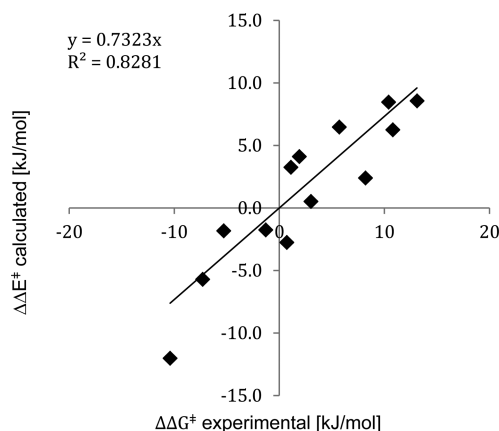


Figure 11. Calculated  $\Delta\Delta E^\ddagger$  vs experimental  $\Delta\Delta G^\ddagger$ .

Table 5. Structures with Experimental ee and  $\Delta\Delta G^\ddagger$  and Calculated  $\Delta\Delta E^\ddagger$

diphosphine	diamine	substrate	% ee expt.	$\Delta\Delta G^\ddagger$ exptl. [kJ/mol]	$\Delta\Delta E^\ddagger$ calcd [kJ/mol]	ref
(R)-BINAP	TMEN	acetophenone	51–55 (R)	2.8–3.1	0.5	18a
(S)-BINAP	(S,S)-DPEN	1-acetylnaphthalene	97 (R)	10.4	8.5	16a
(S)-BINAP	(R,R)-DPEN	1-acetylnaphthalene	14 (R)	0.7	–2.8	16a
(S)-XylBINAP	(S)-DAIPEN	acetophenone	99 (R)	13.1	8.6	16c
(S)-XylBINAP	(S,S)-DPEN	4-methylpent-3-en-2-one	93 (R)	8.2	2.4	16c
(S)-XylBINAP	(S,S)-DPEN	cyclohexylmethylketone	37 (R)	1.9	4.1	18b
(R)-XylBINAP	(R)-DAIPEN	(E)-6-methylhept-2-en-4-one	90 (S)	–7.3	–5.7	16c
(S)-TolBINAP	(R)-DMAPEN	(E)-chalcone	97 (S)	–10.4	–12.0	16d
(S)-TolBINAP	(R,R)-DMDPEN	acetophenone	79 (S)	–5.3	–1.8	16
(S)-TolBINAP	(S,S)-DMDPEN	acetophenone	22 (R)	1.1	3.3	16
(S)-TolBINAP	(S,S)-DPEN	acetophenone	82 (R)	5.7	6.5	16
(S)-TolBINAP	(S,S)-DPEN	2-acetyltoleune	97.5 (R)	10.8	6.3	16b
(R)-TolBINAP	(R,R)-DPEN	2,4,4-trimethylcyclohex-2-enone	26 (S)	–1.3	–1.8	16b



99%. The major envisioned use of the force field would be in virtual screening, where the current accuracy would be sufficient to exclude all proposed catalysts with low selectivity and leave only a handful of promising candidates for experimental testing.

We can use the force field to analyze the major contributing factors in the observed selectivity. From the “lock-and-key” principle, one would expect the major difference between paths to enantiomeric products to lie mainly in nonbonded interactions with the two groups of the ketone. It has previously been noted that a major factor for the classical substrate acetophenone is an attractive interaction between one of the nonreacting N–H bonds and the  $\pi$  system of the aromatic ring.<sup>16,18</sup> This interaction can be seen also in our cases. However, several other factors must also be of importance. One example is the case where (E)-chalcone gives a very high selectivity together with the DMAPEN ligand, despite the fact that both sides of the ketone possess  $\pi$  systems, and no N–H bonds are available for hydrogen bonding. An energy analysis reveals that the major difference between the diastereomeric paths lie in the van der Waals energies, whereas all other interactions (including electrostatics) differ very little. Looking at the shape of the transition states, the tolyl moieties of the diphosphine form a wall-like shape that can form attractive edge–face interactions with both phenyl moieties of the chalcone. However, the tolyl groups of one phosphine moiety are closer to the reaction center than the other. The substrate shows a strong preference for an orientation where the shorter substituent, the phenyl group, interacts with the closer moiety, whereas the longer styryl group easily reaches the tolyl groups of the distal phosphine. Inverting the substrate leads to a geometry with much worse fit between the ketone substituents and the phosphine substituents. This example shows that the interactions responsible for selectivity are very specific to a certain substrate–ligand combination, corroborating the observation that general rules for selectivity are hard to find for this type of catalyst. Thus, the need for a rapid screening method is apparent.

## CONCLUSIONS

We have used the Q2MM method to develop a reaction specific force field for the asymmetric hydrogenation of simple ketones. The Q2MM force field, which is developed from the standard MM3\* force field with modifications solely based on QM calculations, can predict the major enantiomer of the product and continues to demonstrate an excellent level of accuracy. The MUE was 2.7 kJ/mol, fully sufficient for virtual screening aimed at enriching a candidate pool of catalysts. Work on extending this technology to virtual screening and catalyst design is currently ongoing in our laboratories.

## ASSOCIATED CONTENT

### Supporting Information

Cartesian coordinates, imaginary frequencies, SCF energies, and Gibbs free energies for all QM transition state structures; QM input files, including ESP charge determination details; force field parameters in MacroModel format; residual plots for internal validation; experimental and calculated energies for the test set. This material is available free of charge via the Internet at <http://pubs.acs.org>

## AUTHOR INFORMATION

### Corresponding Author

\*E-mail: [pon@chem.gu.se](mailto:pon@chem.gu.se).

### Notes

The authors declare no competing financial interest.

## ACKNOWLEDGMENTS

The research leading to these results has received funding from the European Community's Seventh Framework Programme [FP7/2007-2013] for SYNFLOW under grant agreement No. NMP2-LA-2010-246461, the U.S. National Science Foundation (CHE 1058075 and TG-CHE120050) and the Shenzhen Peacock Program (KQTD201103)

## REFERENCES

- (1) (a) Ohno, K.; Maeda, S. *J. Mol. Catal. A* **2010**, 324, 133–140. (b) Maeda, S.; Morokuma, K. *J. Chem. Theory Comput.* **2011**, 7, 2335–2345.
- (2) (a) Oslob, J. D.; Åkermar, B.; Helquist, P.; Norrby, P.-O. *Organometallics* **1997**, 16, 3015–3021. (b) Kozłowski, M. C.; Ianni, J. C. *J. Mol. Catal. A* **2010**, 324, 141–145. (c) Fey, N.; Orpen, A. G.; Harvey, J. N. *Coord. Chem. Rev.* **2009**, 253, 704–722. (d) Harper, K. C.; Sigman, M. S. *Science* **2011**, 333, 1875–1878.
- (3) Eksterowicz, J. E.; Houk, K. N. *Chem. Rev.* **1993**, 93, 2439–2461.
- (4) Åqvist, J.; Warshel, A. *Chem. Rev.* **1993**, 93, 2523–2544.
- (5) Brown, J. M.; Deeth, R. J. *Angew. Chem., Int. Ed.* **2009**, 48, 4476–4479.
- (6) Corbeil, C. R.; Moitessier, N. *J. Mol. Catal. A* **2010**, 324, 146–155.
- (7) Balcells, D.; Maseras, F. *New J. Chem.* **2007**, 31, 333–343.
- (8) (a) van Duin, A. C. T.; Dasgupta, S.; Lorant, F.; Goddard, W. A., III. *J. Phys. Chem. A* **2001**, 105, 9396–9409. (b) Kim, Y.; Corchado, J. C.; Villa, J.; Xing, J.; Truhlar, D. G. *J. Chem. Phys.* **2000**, 112, 2718–2735. (c) Rappe, A. K.; Pietsch, M. A.; Wiser, D. C.; Hart, J. R.; Bormann, L. M.; Skiff, W. M. *Mol. Eng.* **1997**, 7, 385–400.
- (9) Jensen, F. *J. Chem. Phys.* **2003**, 119, 8804–8808.
- (10) Weill, N.; Corbeil, C. R.; De Schutter, J. W.; Moitessier, N. *J. Comput. Chem.* **2011**, 32, 2878–2889.
- (11) Norrby, P.-O. In *Transition State Modeling for Catalysis*; Truhlar, D. G., Morokuma, K., Eds.; ACS Symposium Series 721, American Chemical Society: Washington, DC, 1999; pp 163–172.
- (12) Jensen, F.; Norrby, P.-O. *Theor. Chem. Acc.* **2003**, 109, 1–7.
- (13) Nilsson Lill, S. O.; Forbes, A.; Donoghue, P.; Verdolino, V.; Wiest, O.; Rydberg, P.; Norrby, P.-O. *Curr. Org. Chem.* **2010**, 14, 1629–1645.
- (14) (a) Norrby, P.-O.; Rasmussen, T.; Haller, J.; Strassner, T.; Houk, K. N. *J. Am. Chem. Soc.* **1999**, 121, 10186–10192. (b) Fristrup, P.; Tanner, D.; Norrby, P.-O. *Chirality* **2003**, 15, 360–368. Fristrup, P.; Jensen, G. H.; Andersen, M. L. N.; Tanner, D.; Norrby, P.-O. *J. Organomet. Chem.* **2006**, 691, 2182–2198.
- (15) (a) Donoghue, P. J.; Helquist, P.; Norrby, P.-O.; Wiest, O. *J. Chem. Theory Comput.* **2008**, 4, 1313–1323. (b) Donoghue, P. J.; Helquist, P.; Norrby, P.-O.; Wiest, O. *J. Am. Chem. Soc.* **2009**, 131, 410–411.
- (16) (a) Ohkuma, T.; Ooka, H.; Hashiguchi, S.; Ikariya, T.; Noyori, R. *J. Am. Chem. Soc.* **1995**, 117, 2675–2676. (b) Ohkuma, T.; Doucet, H.; Pham, T.; Mikami, K.; Korenaga, T.; Terada, M.; Noyori, R. *J. Am. Chem. Soc.* **1998**, 120, 1086–1087. (c) Ohkuma, T.; Koizumi, M.; Doucet, H.; Pham, T.; Kozawa, M.; Murata, K.; Katayama, E.; Yokozawa, T.; Ikariya, T.; Noyori, R. *J. Am. Chem. Soc.* **1998**, 120, 13529–13530. (d) Noyori, R.; Ohkuma, T. *Angew. Chem., Int. Ed.* **2001**, 40, 40–73. (e) Sandoval, C. A.; Ohkuma, T.; Muniz, K.; Noyori, R. *J. Am. Chem. Soc.* **2003**, 125, 13490–13503.
- (17) Ooka, H.; Arai, N.; Azuma, K.; Kurono, N.; Ohkuma, T. *J. Org. Chem.* **2008**, 73, 9084–9093.
- (18) (a) Abdur-Rashid, K.; Clapham, S. E.; Hadzovic, A.; Harvey, J. N.; Lough, A. J.; Morris, R. H. *J. Am. Chem. Soc.* **2002**, 124, 15104–



15118. (b) Di Tommaso, D.; French, S. A.; Zanotti-Gerosa, A.; Hancock, F.; Palin, E. J.; Catlow, C. R. A. *Inorg. Chem.* **2008**, *47*, 2674–2687. (c) Leyssens, T.; Peeters, D.; Harvey, J. N. *Organometallics* **2008**, *27*, 1514–1523. (d) Iuliis, M. Z. D.; Morris, R. H. *J. Am. Chem. Soc.* **2009**, *131*, 11263–11269. (e) Chen, H. Y. T.; Di Tommaso, D.; Hogarth, G.; Catlow, C. R. A. *Catal. Lett.* **2011**, *141*, 1761–1766.
- (19) Dub, P. A.; Henson, N. J.; Martin, R. L.; Gordon, J. C. *J. Am. Chem. Soc.* **2014**, *136*, 3505–3521.
- (20) Abdur-Rashid, K.; Faatz, M.; Lough, A. J.; Morris, R. H. *J. Am. Chem. Soc.* **2001**, *123*, 7473–7474.
- (21) Norrby, P.-O. *J. Mol. Struct.: THEOCHEM* **2000**, *506*, 9–16.
- (22) (a) Becke, A. D. *J. Chem. Phys.* **1993**, *98*, 5648–5652. (b) Lee, C. T.; Yang, W. T.; Parr, R. G. *Phys. Rev. B* **1988**, *37*, 785–789. (c) Stephens, P. J.; Devlin, F. J.; Chabalowski, C. F.; Frisch, M. J. *J. Phys. Chem.* **1994**, *98*, 11623–11627.
- (23) *Jaguar*, version 7.9; Schrödinger, LLC: New York, 2011. For recent versions, see: [www.schrodinger.com](http://www.schrodinger.com).
- (24) Hay, P. J.; Wadt, W. R. *J. Chem. Phys.* **1985**, *82*, 299–310.
- (25) (a) Chirlian, L. E.; Francel, M. M. *J. Comput. Chem.* **1987**, *8*, 894–905. (b) Woods, R. J.; Khalil, M.; Pell, W.; Moffat, S. H.; Smith, V. H., Jr. *J. Comput. Chem.* **1990**, *11*, 297–310. (c) Breneman, C. M.; Wiberg, K. B. *J. Comput. Chem.* **1990**, *11*, 361–373.
- (26) Norrby, P.-O.; Brandt, P. *Coord. Chem. Rev.* **2001**, *212*, 79–109.
- (27) Maple, J. R.; Hwang, M. J.; Stockfisch, T. P.; Dinur, U.; Waldman, M.; Ewig, C. S.; Hagler, A. T. *J. Comput. Chem.* **1994**, *15*, 162–182.
- (28) Norrby, P.-O.; Liljefors, T. *J. Comput. Chem.* **1998**, *19*, 1146–1166.
- (29) Chang, G.; Guida, W. C.; Still, W. C. *J. Am. Chem. Soc.* **1989**, *111*, 4379–4386.
- (30) Kolossváry, I.; Guida, W. C. *J. Am. Chem. Soc.* **1996**, *118*, 5011–5019.
- (31) *MacroModel*, version 9.9; Schrödinger, LLC: New York, 2012. For recent versions, see: [www.schrodinger.com](http://www.schrodinger.com).
- (32) Allinger, N. L.; Yuh, Y. H.; Li, J. H. *J. Am. Chem. Soc.* **1989**, *111*, 8551–8566.
- (33) Allinger, N. L.; Zhou, X. F.; Bergsma, J. *J. Mol. Struct.: THEOCHEM* **1994**, *118*, 69–83.
- (34) Norrby, P.-O.; Wärnmark, K.; Åkermark, B.; Moberg, C. *J. Comput. Chem.* **1995**, *16*, 620–627.